Research Square

Preprints are preliminary reports that have not undergone peer review.
They should not be considered conclusive, used to inform clinical practice,
or referenced by the media as validated information.

Initial Conformation Governs Amyloid-β42 Dynamics and Association at a POPC Membrane-Water Interface

Yersultan Arynbek

yersultan@jinr.ru

Joint Institute for Nuclear Research

Khlood A.A.A. Abdeljawaad

Joint Institute for Nuclear Research

Duc Huy Le

Joint Institute for Nuclear Research

Kahramon Mamatkulov

Joint Institute for Nuclear Research

Grigory Arzumanyan

Joint Institute for Nuclear Research

Research Article

Keywords: Amyloid-β42, Molecular dynamics, POPC membrane, Conformational dynamics, Membrane association, Structural polymorphism

Posted Date: September 12th, 2026

DOI: https://doi.org/10.21203/rs.3.rs-10818226/v1

License: This work is licensed under a Creative Commons Attribution 4.0 International License.
Read Full License

Additional Declarations: No competing interests reported.

Initial Conformation Governs Amyloid-β42 Dynamics and Association at a POPC Membrane-Water Interface

Yersultan Arynbek [1,2,3,*], Khlood A. A. Abdeljawaad [1,4,5], Huy Le Duc [1,6,7], Kahramon Mamatkulov [1], Grigory Arzumanyan [1]

[1] *Department of Raman Spectroscopy, Frank Laboratory of Neutron Physics, Joint Institute for Nuclear Research, Dubna, Russia*

[2] *Faculty of Physics and Technology, al-Farabi Kazakh National University, Almaty, Kazakhstan*

[3] *Institute of Nuclear Physics, Almaty, Kazakhstan*

[4] *Academy of Scientific Research & Technology (ASRT), Cairo, Egypt*

[5] *Chemistry Department, Faculty of Science, Minia University, Minia, Egypt*

[6] *Institute of Physics, Vietnam Academy of Science and Technology, Hanoi, Vietnam*

[7] *Graduate University of Science and Technology, Vietnam Academy of Science and Technology, Hanoi, Vietnam*

* Corresponding author: yersultan@jinr.ru

Yersultan Arynbek: http://orcid.org/0000-0002-6942-8211

Khlood A. A. Abdeljawaad: http://orcid.org/0000-0001-8667-664X

Huy Le Duc: http://orcid.org/0009-0004-6574-6935

Kahramon Mamatkulov: http://orcid.org/0000-0001-7503-9362

Grigory Arzumanyan: http://orcid.org/0000-0002-8755-0747

Abstract

The conformational heterogeneity of amyloid-β42 (Aβ42) may influence its early interactions with lipid membranes, yet the extent to which different initial structures determine subsequent membrane association remains unclear. Here, three nuclear magnetic resonance (NMR) derived Aβ42 monomer structures (1IYT, 1Z0Q, and 6SZF) were examined at a 1-palmitoyl-2-oleoyl-sn-phosphocholine (POPC) membrane-water interface. Despite an identical environment, the monomers followed different trajectories during comparative 200-ns all-atom molecular dynamics simulations using the CHARMM36m force field. The predominantly α-helical 1IYT structure underwent substantial relaxation, with α-helical content decreasing from 78.57% to 44.77%. The 1Z0Q monomer exhibited extensive rearrangement, developing 18.45% π-helical structure. In contrast, the fibril-derived 6SZF structure remodeled toward an α-helical state, increasing from 11.90% to 41.59%. Structural evolution and membrane association were evaluated using root-mean-square deviation (RMSD), fluctuation (RMSF), radius of gyration, peptide-membrane distance, interfacial contacts, hydrogen bonding, and secondary-structure analysis. These findings demonstrate that the initial conformational state of Aβ42 strongly influences its structural response to a common lipid-water environment and emphasize the importance of starting-structure selection when modeling early amyloid-membrane interactions.

Keywords: Amyloid-β42; Molecular dynamics; POPC membrane; Conformational dynamics; Membrane association; Structural polymorphism

1. Introduction

Alzheimer's disease (AD) is a progressive neurodegenerative disorder characterized by multiple pathological alterations, among which the accumulation of amyloid-β (Aβ) peptides remains one of the most extensively investigated molecular features. Aβ peptides are generated through sequential proteolytic processing of the amyloid precursor protein, with Aβ40 and Aβ42 representing two major isoforms. The additional two hydrophobic residues at the C-terminus of Aβ42 increase its propensity for conformational rearrangement, self-association, and aggregation compared with the shorter Aβ40 isoform [Hardy and Selkoe 2002; Selkoe and Hardy 2016]. Although mature amyloid fibrils constitute a characteristic pathological feature of AD, considerable evidence indicates that earlier soluble Aβ species and their interactions with cellular components are highly relevant to amyloid-associated toxicity. In this context, the interaction of Aβ with lipid membranes has received particular attention because the membrane surface can influence peptide localization, conformation, and assembly, while membrane-associated Aβ species can reciprocally perturb lipid organization and membrane integrity [Butterfield and Lashuel 2010; Matsuzaki 2007; Williams and Serpell 2011]. Lipid bilayers should therefore not be regarded simply as passive boundaries surrounding amyloidogenic peptides. Membrane surfaces create heterogeneous physicochemical environments containing aqueous, polar interfacial, and hydrophobic regions that can differentially stabilize peptide conformations. Association with these interfaces can alter peptide orientation, local concentration, secondary structure, and intermolecular interactions, potentially affecting subsequent aggregation pathways [Butterfield and Lashuel 2010; Matsuzaki 2007; Williams and Serpell 2011]. Experimental and computational investigations have consequently described several possible modes of Aβ-membrane interaction, including transient surface association, persistent adsorption, partial insertion, deeper

64 penetration of selected peptide regions, and membrane-associated conformational rearrangement [Davis and
65 Berkowitz 2009; Sciacca et al. 2012; Tofoleanu and Buchete 2012; Williams and Serpell 2011]. The balance among these behaviors
66 depends on several variables, including peptide aggregation state, lipid composition, membrane charge,
67 cholesterol and ganglioside content, ionic environment, and the structural state of the peptide before
68 membrane encounter [Abdeljawaad et al. 2026; Davis and Berkowitz 2009; Esawii et al. 2025; Mamatkulov et al. 2025; Sciacca et al. 2012;
69 Tofoleanu and Buchete 2012; Williams and Serpell 2011].

70 Aβ42 presents a particular challenge because of its pronounced conformational heterogeneity
71 [Mrdenovic et al. 2022; Nguyen and Derreumaux 2023]. The monomer does not possess a single universally stable native
72 structure in solution; instead, it can populate different conformational ensembles depending on its
73 molecular environment. Experimental structural studies provide direct evidence of this plasticity. Nuclear
74 magnetic resonance (NMR) spectroscopy of Aβ42 in an apolar membrane-mimetic environment yielded
75 the structure deposited as PDB 1IYT, characterized by extensive α-helical organization [Crescenzi et al. 2002;
76 Davis and Berkowitz 2009]. In contrast, the aqueous-solution NMR structure represented by PDB 1Z0Q describes
77 a substantially different conformational ensemble of the same 42-residue sequence [Tomaselli et al. 2006]. At
78 the other end of the amyloid structural landscape, high-resolution cryo-electron microscopy (cryo-EM)
79 has resolved the highly ordered architecture adopted by Aβ42 within mature fibrillar assemblies,
80 including the structure represented by PDB 6SZF [Santoro et al. 2021]. These experimentally derived structures
81 therefore capture markedly different regions of the accessible Aβ42 conformational landscape and
82 provide structurally distinct starting points for examining peptide behavior under a common membrane
83 environment. Model lipid bilayers offer a controlled platform for separating fundamental peptide-lipid
84 interactions from the considerable compositional complexity of biological membranes.
85 Phosphatidylcholine is a major zwitterionic phospholipid class, and 1-palmitoyl-2-oleoyl-sn-glycero-3-
86 phosphocholine (POPC) forms fluid bilayers under physiological-temperature conditions. A POPC

bilayer therefore provides a useful reference environment for investigating how Aβ42 responds to a neutral phosphatidylcholine membrane-water interface without simultaneously introducing strong electrostatic effects from anionic lipids or specific interactions associated with cholesterol and gangliosides. Such a simplified system does not reproduce the complete composition of neuronal membranes; rather, it enables controlled analysis of fundamental peptide-bilayer interactions against a well-defined lipid background. More complex membranes containing cholesterol, sphingomyelin, GM1, and charged phospholipids can subsequently be used to evaluate composition-specific effects. Previous molecular simulation studies have demonstrated that Aβ-membrane interactions are highly sensitive to both peptide state and membrane composition. Atomistic and enhanced-sampling simulations have reported surface adsorption, partial insertion, conformational transitions, and lipid perturbation for Aβ monomers and oligomeric species in phosphatidylcholine-containing and more complex membrane systems (Banerjee et al. 2020; Davis and Berkowitz 2009; Poojari et al. 2013; Tofoleanu and Buchete 2012; Weber and Uversky 2017). These studies have established that membrane association cannot be represented by a single universal binding geometry. Instead, Aβ can sample multiple interfacial states whose stability depends on the molecular characteristics of both the peptide and the lipid environment. Importantly, simulations in which Aβ42 is initially located in the aqueous phase have shown that membrane encounter itself can be accompanied by substantial structural rearrangement, emphasizing the dynamic nature of the peptide-membrane interface (Poojari et al. 2013). Despite these advances, the influence of the initial Aβ42 conformational state remains an important methodological consideration.

Molecular dynamics (MD) trajectories necessarily begin from a defined molecular configuration, whereas intrinsically disordered and conformationally heterogeneous peptides exist as ensembles of interconverting structures. Within computationally accessible timescales, a trajectory may retain elements of its initial structural organization, undergo partial relaxation, or transition toward substantially

different states. Consequently, simulations initiated from a single Aβ42 structure may sample only a subset of the peptide's possible membrane-associated behavior. This issue is especially relevant when experimentally derived starting structures originate from substantially different environments, such as aqueous solution, membrane-mimetic media, or fibrillar assemblies. A controlled comparison of distinct experimentally determined conformations of the same peptide provides one strategy for examining this initial-state dependence. By maintaining peptide sequence, lipid composition, ionic strength, force field, temperature, pressure, and simulation protocol while varying the starting Aβ42 structure, differences among trajectories can be evaluated in relation to the initial conformational state. Such an approach does not imply that a single trajectory exhaustively represents the equilibrium ensemble of each conformer. Rather, it provides a comparative framework for determining whether structurally different starting states exhibit distinct patterns of relaxation, membrane association, and secondary-structure evolution over an equivalent observation period. This distinction is particularly important for the interpretation and reproducibility of MD studies involving conformationally heterogeneous biomolecules. All-atom MD simulations are well suited to such comparisons because they provide simultaneous access to structural and interfacial descriptors that are difficult to resolve experimentally at equivalent temporal and spatial resolution. Backbone root-mean-square deviation (RMSD) and per-residue root-mean-square fluctuation (RMSF) characterize global structural evolution and local flexibility, whereas the radius of gyration provides information on peptide compactness. Peptide-membrane distances, intermolecular contacts, and hydrogen-bonding patterns can be used to follow association with the lipid interface, while time-resolved secondary-structure analysis enables identification of changes in helical, β-structured, and disordered regions. The CHARMM36m force field is particularly relevant in this context because it was developed to improve the description of backbone conformational ensembles for both folded proteins and intrinsically disordered peptides and proteins [(Huang et al. 2017)]. Standardized system-building frameworks

such as CHARMM-GUI additionally facilitate transparent and reproducible preparation of membrane-containing simulation systems (Jo et al. 2008; Jo et al. 2009).

In the present study, comparative 200-ns all-atom MD simulations were performed for three experimentally derived Aβ42 monomer structures—1IYT, 1Z0Q, and 6SZF—in the presence of the same zwitterionic POPC bilayer. In each system, the peptide was initially positioned in the aqueous phase adjacent to the upper membrane leaflet rather than being pre-inserted into the lipid bilayer. This configuration enabled the spontaneous approach of each monomer toward the membrane-water interface and allowed its subsequent association behavior and conformational response to be monitored under equivalent simulation conditions. Structural evolution was evaluated using complementary analyses of RMSD, RMSF, radius of gyration, peptide-membrane distance, interfacial contacts, hydrogen bonding, and secondary structure. By comparing structurally distinct experimental starting models within an otherwise consistent computational framework, the study aims to determine how the initial conformational state influences the early structural dynamics and membrane-association behavior of monomeric Aβ42 at a POPC membrane-water interface.

2. Computational Methodology

2.1. Selection and preparation of Aβ42 starting structures

Three experimentally derived structures of full-length amyloid-β42 (Aβ42) were selected from the Protein Data Bank (PDB) to represent distinct initial conformational states: 1IYT, 1Z0Q, and 6SZF (Berman et al. 2000; Crescenzi et al. 2002; Santoro et al. 2021; Tomaselli et al. 2006). The 1IYT structure was determined by solution nuclear magnetic resonance (NMR) spectroscopy in an apolar environment and represents a predominantly α-helical Aβ42 conformation. The 1Z0Q structure was derived from solution NMR measurements under highly aqueous conditions and exhibits substantially different conformational

organization. For 6SZF, a single Aβ42 chain comprising residues 1-42 was extracted from the experimentally determined fibrillar assembly and used as a monomeric starting configuration. The same 42-residue Aβ sequence was retained in all three systems, such that the experimentally derived initial three-dimensional conformation represented the principal structural variable among the simulations. Before membrane-system construction, each structure was inspected for residue completeness and prepared using the CHARMM-GUI workflow.

2.2. Construction of the Aβ42-POPC systems

Three independent peptide-membrane systems were constructed using CHARMM-GUI, with an identical membrane composition and solution environment applied to each Aβ42 starting structure (Jo et al. 2008). Each membrane consisted of 192 molecules of 1-palmitoyl-2-oleoyl-sn-glycero-3-phosphocholine (POPC), symmetrically distributed between the two leaflets, with 96 POPC molecules in the upper leaflet and 96 in the lower leaflet. Importantly, the Aβ42 monomers were not initially embedded within the lipid bilayer. In each system, one Aβ42 monomer was positioned in the aqueous phase above the upper POPC leaflet. This configuration was selected to examine the behavior of structurally distinct Aβ42 conformations in the presence of the same membrane-water interface without imposing a predefined membrane-bound or membrane-inserted configuration. Each system was solvated with explicit TIP3P water, and NaCl was added to neutralize the system and establish an ionic concentration of 0.15 M (Jorgensen et al. 1983). Periodic boundary conditions were applied in all three spatial dimensions.

2.3. Energy minimization and equilibration

All molecular dynamics simulations were performed using GROMACS 2024.5 with the CHARMM36m force field and the corresponding CHARMM lipid parameters [(Abraham et al. 2015; Huang et al. 2017)]. Prior to equilibration, each system was subjected to energy minimization using the steepest-descent algorithm for a maximum of 5,000 steps, with a convergence criterion of 1,000 kJ mol^{-1} nm^{-1}. A Verlet cutoff scheme was employed with a neighbor-list cutoff of 1.2 nm. Long-range electrostatic interactions were calculated using the particle mesh Ewald (PME) method with a real-space Coulomb cutoff of 1.2 nm [(Simmonett and Brooks 2021)]. Van der Waals interactions were treated using a force-switching scheme between 1.0 and 1.2 nm. Bonds involving hydrogen atoms were constrained using the LINCS algorithm [(Hess et al. 1997)]. Position restraints on peptide and lipid components were maintained during minimization according to the CHARMM-GUI-generated protocol. Energy minimization was followed by the standard multistep equilibration protocol generated by CHARMM-GUI, during which positional restraints were progressively reduced to allow gradual relaxation of the peptide, lipid bilayer, solvent, and ions. The equilibrated systems were subsequently used as starting configurations for the production MD simulations.

2.4. Production molecular dynamics simulations

Following equilibration, production MD simulations were performed for a total of 200 ns for each Aβ42-POPC system. The CHARMM-GUI production workflow was executed as sequential 1-ns simulation segments, with each new segment continuing from the coordinates and checkpoint information generated by the preceding segment. Two hundred consecutive production segments were therefore used to generate a continuous 200-ns trajectory for each system. Production trajectories were propagated using the leap-frog integration algorithm with a time step of 2 fs. The simulations were

conducted in the NPT ensemble under periodic boundary conditions. Temperature was maintained at 310.15 K using the velocity-rescaling (v-rescale) thermostat with a coupling constant of 1.0 ps [Bussi et al. 2007]. The solute, membrane, and solvent were assigned to separate temperature-coupling groups. Pressure was maintained at 1 bar using the C-rescale barostat with semi-isotropic pressure coupling, allowing the dimensions parallel to the membrane plane and along the membrane normal to respond independently [Bernetti and Bussi 2020]. A pressure-coupling constant of 5.0 ps and compressibility of 4.5×10^{-5} bar^{-1} were applied. Long-range electrostatic interactions were evaluated using the PME method, with the real-space Coulomb cutoff set to 1.2 nm. Van der Waals interactions were treated using a force-switching scheme over the range of 1.0-1.2 nm, and the neighbor-list cutoff was set to 1.2 nm using the Verlet cutoff scheme. Bonds involving hydrogen atoms were constrained using the LINCS algorithm. Coordinates were written every 100 ps for subsequent trajectory analysis. Thus, the three systems were simulated using the same membrane composition, solvent environment, ionic strength, force field, temperature, pressure, and MD protocol, while differing in the experimentally derived initial conformation of the Aβ42 monomer. All computations were held on the basis of the HybriLIT heterogeneous computing platform (LIT, JINR) [Anikina et al. 2025].

2.5. Trajectory analysis

The 200-ns production trajectories were analyzed to compare the structural dynamics and membrane-association behavior of the three Aβ42 conformers. Root-mean-square deviation (RMSD) of the peptide backbone was calculated to evaluate the overall conformational evolution of Aβ42 during the simulations, while root-mean-square fluctuation (RMSF) was used to characterize residue-specific flexibility [Benson and Daggett 2008; Maiorov and Crippen 1994]. Changes in peptide compactness were assessed using the radius of gyration (Rg) [Torrens-Fontanals et al. 2020]. The evolution of Aβ42 secondary structure was

evaluated using DSSP analysis, allowing changes in α-helical, β-sheet, π-helical, turn, bend, and coil conformations to be monitored throughout the trajectories [(Gorelov et al. 2024)]. Secondary-structure populations were compared among the three starting structures and over the course of the 200-ns simulations. Peptide-membrane association was characterized by monitoring the distance between Aβ42 and the POPC bilayer as a function of simulation time. Interactions at the membrane-water interface were further examined through peptide-lipid contact and hydrogen-bond analyses, providing complementary information on the extent and persistence of peptide association with the POPC surface. Together, these analyses were used to compare the conformational stability, structural remodeling, flexibility, compactness, and membrane-association behavior of the 1IYT-, 1Z0Q-, and 6SZF-derived Aβ42 monomers under identical simulation conditions [(Bundschuh et al. 2026; Kabsch and Sander 1983)]. Data post-processing and visualization were performed using VMD and custom scripts written in Python programming language, version 3.10 [Python Software Foundation, 2021] [(Humphrey et al. 1996)].

3. Results and Discussion

3.1. Comparative simulation design and initial Aβ42 conformations

Three experimentally derived Aβ42 structures, 1IYT, 1Z0Q, and 6SZF, were selected to represent distinct initial conformational states of the same 42-residue peptide (Fig. 1A-C). The structures differ substantially in their initial secondary-structure organization, providing contrasting starting configurations for evaluating Aβ42 dynamics in a common membrane environment. Importantly, the purpose of the comparison was not to reproduce the experimental environments from which these structures were originally determined, but rather to examine how structurally distinct Aβ42 starting states behave when subjected to identical simulation conditions. For each system, a single Aβ42 monomer was positioned in the aqueous phase above the upper leaflet of a POPC bilayer containing 192 lipid molecules

(96 per leaflet) (Fig. 1d). The peptide was therefore not initially embedded within the membrane. This common starting geometry allowed the subsequent peptide-membrane encounter and conformational evolution to occur during the 200-ns trajectories without imposing a predefined membrane-inserted configuration. By maintaining the peptide sequence, membrane composition, solvent environment, ionic strength, force field, temperature, pressure, and simulation protocol while varying the experimentally derived starting conformation, the three systems provide a controlled comparative framework for examining the relationship between initial Aβ42 structure, conformational remodeling, and membrane-association behavior.

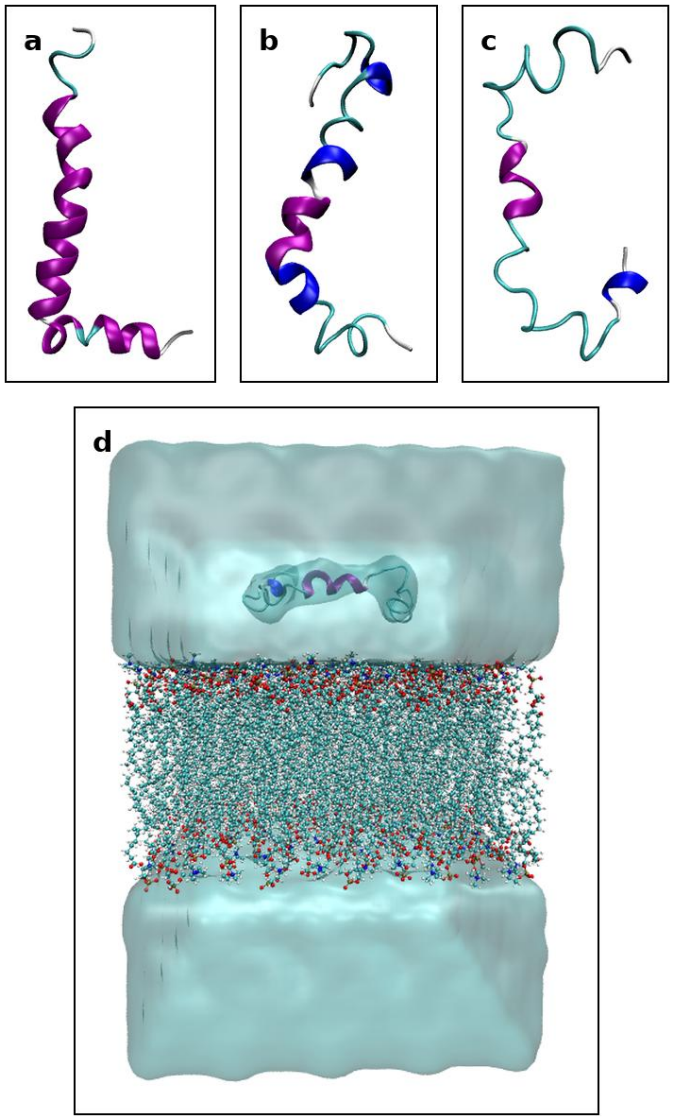


Fig. 1 Experimentally derived Aβ42 structures used as starting conformations for the molecular dynamics simulations: (A) 1IYT, (B) 1Z0Q, and (C) 6SZF. (D) Representative simulation system showing Aβ42 initially positioned in the aqueous phase above the upper leaflet of a POPC bilayer

3.2. Global conformational dynamics and structural compactness of Aβ42

The conformational dynamics of the three Aβ42 models were evaluated throughout the 200-ns simulations to determine how their distinct starting structures influenced their subsequent behavior in the

POPC-water environment. Global structural deviation, residue-specific flexibility, and molecular compactness were assessed using root-mean-square deviation (RMSD), root-mean-square fluctuation (RMSF), and radius of gyration (Rg), respectively. These complementary descriptors provide information on different aspects of peptide dynamics and were therefore considered together when evaluating the conformational behavior of the three systems.

3.2.1. Root-mean-square deviation (RMSD) analysis

The backbone RMSD profiles revealed distinct conformational trajectories for the 1IYT-, 1Z0Q-, and 6SZF-derived Aβ42 systems over the 200-ns simulations (Fig. 2). All three systems deviated substantially from their respective starting structures, although the magnitude and temporal pattern of these deviations differed considerably. For 1IYT, the RMSD increased progressively during the early part of the trajectory and reached approximately 1.0-1.1 nm within the first 40-50 ns. This was followed by pronounced fluctuations and a temporary reduction in RMSD during the intermediate portion of the simulation. A marked change occurred at approximately 125 ns, after which RMSD increased rapidly and remained predominantly around 1.2-1.4 nm for the remainder of the trajectory. The persistence of these higher values suggests that 1IYT underwent substantial conformational reorganization and subsequently sampled a structural state markedly different from its initial configuration. The 1Z0Q system exhibited a different dynamic profile. RMSD increased rapidly during the first approximately 30-40 ns, reaching values close to 1.0-1.1 nm. Thereafter, the trajectory was characterized by repeated fluctuations, with RMSD predominantly distributed around 0.8-1.0 nm. Several transient structural rearrangements were evident throughout the simulation, but, unlike 1IYT, no sustained late-stage increase was observed. Instead, RMSD decreased during the final portion of the trajectory, approaching approximately 0.7 nm near 200 ns. This behavior indicates continued conformational rearrangement

throughout the simulation while maintaining a lower overall deviation from the starting configuration during the later stages compared with 1IYT. For 6SZF, a rapid increase in RMSD was also observed during the early simulation. The deviation subsequently increased further and reached approximately 1.2-1.3 nm during the middle portion of the trajectory. These relatively high values persisted for an extended period before gradually decreasing after approximately 150 ns. During the final part of the simulation, RMSD generally fluctuated around 1.0-1.1 nm. The substantial deviation observed for 6SZF indicates extensive reorganization of the fibril-derived monomer after its introduction into the POPC-water environment. Overall, the RMSD analysis demonstrates that the three Aβ42 starting conformations followed distinct structural pathways despite being simulated under identical environmental conditions. 1IYT exhibited a pronounced late-stage conformational transition, 1Z0Q showed persistent but comparatively moderate structural fluctuations, and 6SZF underwent extensive early and intermediate reorganization followed by a partial reduction in deviation during the later trajectory. Importantly, higher RMSD values should not be interpreted directly as reduced structural stability, particularly for a conformationally dynamic peptide such as Aβ42. RMSD quantifies deviation from the initial coordinates rather than thermodynamic stability; therefore, the observed changes are interpreted here primarily as evidence of conformational remodeling. Their structural significance is further evaluated through RMSF, Rg, and secondary-structure analyses in the following sections.

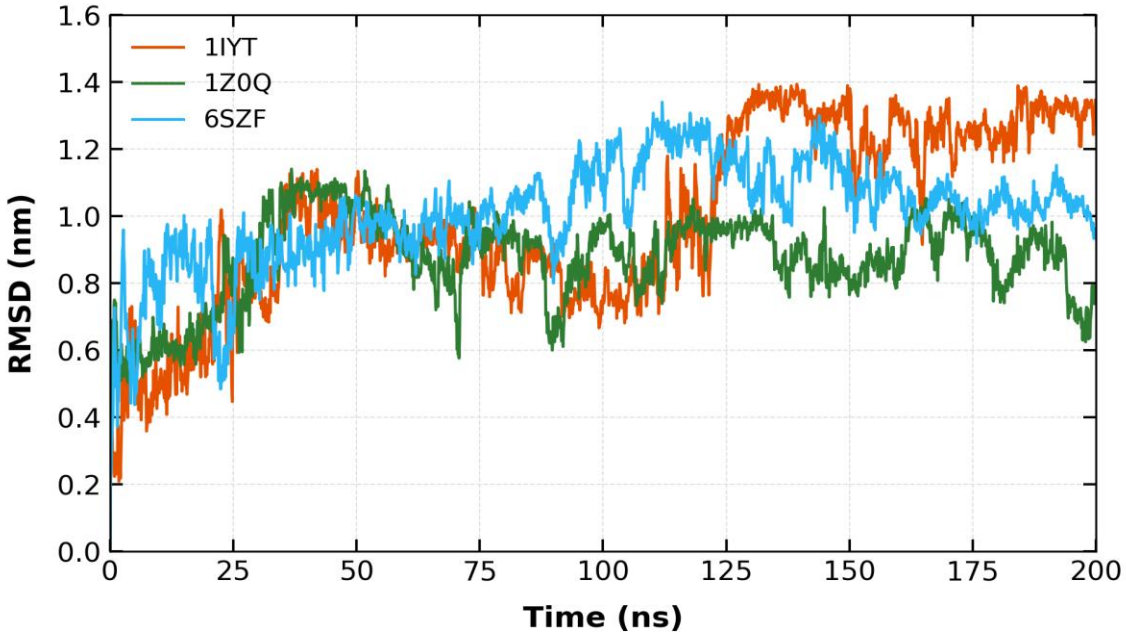


Fig. 2 Backbone RMSD profiles of Aβ42 during the 200-ns molecular dynamics simulations for 1IYT (orange), 1Z0Q (green), and 6SZF (cyan) systems relative to their respective starting structures

3.2.2. Root-mean-square fluctuation (RMSF) analysis

Residue-specific flexibility of Aβ42 was evaluated using root-mean-square fluctuation (RMSF) analysis over the complete 200-ns trajectories (Fig. 3). In contrast to RMSD, which describes the overall deviation of the peptide from its starting structure, RMSF provides information on the local mobility of individual residues. The three systems displayed clearly different fluctuation profiles, indicating that the conformational rearrangements observed during the simulations were distributed nonuniformly along the Aβ42 sequence. The 1IYT-derived peptide exhibited pronounced flexibility at the N-terminal region, where the highest fluctuations were observed. Following this highly mobile segment, RMSF values decreased across much of the central portion of the sequence, although several local increases in mobility remained evident. Flexibility increased again toward the C-terminal region, demonstrating that the structural dynamics of 1IYT were concentrated primarily at the terminal and selected intermediate

regions rather than being uniformly distributed across the peptide. The 1Z0Q system generally displayed a more restricted fluctuation profile. Although the N-terminal residues remained comparatively mobile, the magnitude of their fluctuations was lower than that observed for 1IYT and 6SZF. Much of the central and C-terminal sequence exhibited relatively modest RMSF values, with only localized increases in flexibility. This comparatively restricted residue-level mobility is consistent with the absence of the pronounced sustained late-stage RMSD increase observed for 1IYT, although the RMSD trajectory demonstrates that 1Z0Q still underwent considerable global conformational rearrangement during the simulation. The 6SZF-derived peptide showed substantial residue-dependent mobility. Pronounced fluctuations were observed at the N-terminus, followed by lower mobility across much of the central region. Flexibility subsequently increased toward the C-terminal portion of the sequence, with the terminal residues exhibiting some of the largest fluctuations within this system. The resulting profile indicates that conformational rearrangement of the 6SZF-derived monomer involved substantial mobility of both terminal regions while parts of the central sequence remained comparatively constrained. Comparison of the three profiles therefore identifies the terminal regions, particularly the N-terminus, as major contributors to Aβ42 flexibility, while substantial portions of the central sequence exhibited comparatively restricted mobility. At the same time, the magnitude and distribution of these fluctuations differed among 1IYT, 1Z0Q, and 6SZF, demonstrating that the initial conformational state influenced the residue-level dynamics sampled during the 200-ns simulations. These local differences complement the global rearrangements identified by RMSD and provide a residue-resolved view of the distinct conformational pathways followed by the three Aβ42 models.

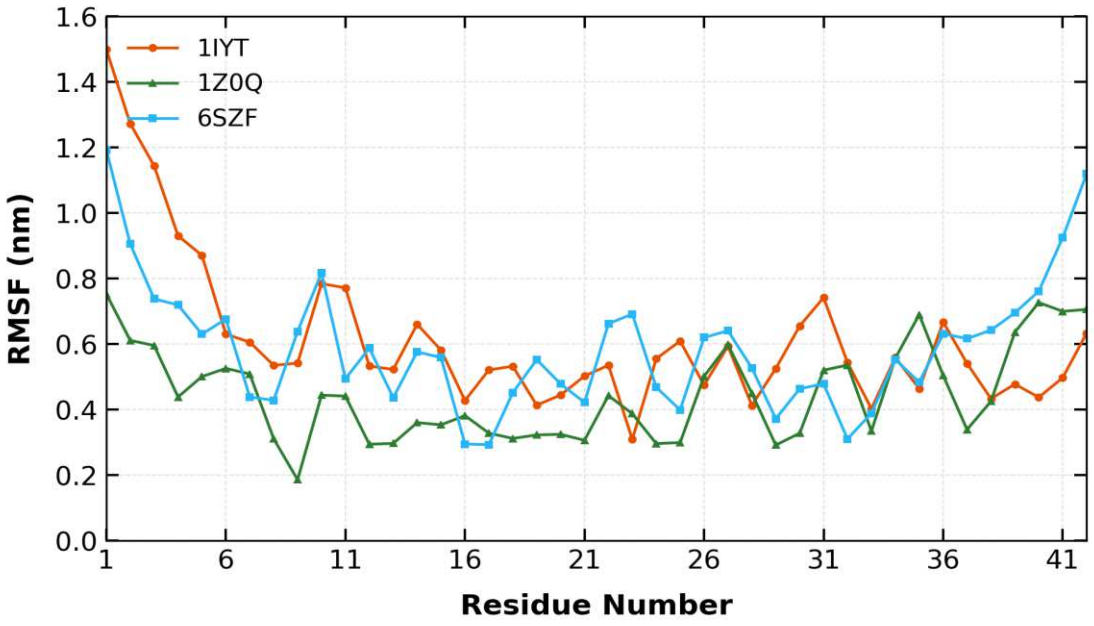


Fig. 3 Residue-wise RMSF profiles of Aβ42 during the 200-ns molecular dynamics simulations for 1IYT (orange), 1Z0Q (green), and 6SZF (cyan) systems calculated over the complete 200-ns trajectories

3.2.3. Radius of gyration (Rg) analysis

The radius of gyration (Rg) was analyzed throughout the 200-ns trajectories to evaluate differences in the global compactness of the three Aβ42 conformers (Fig. 4). In contrast to RMSD, which quantifies structural deviation from a reference configuration, Rg reflects the spatial distribution of the peptide around its center of mass and therefore provides a complementary measure of conformational expansion and compaction. The three systems exhibited markedly different Rg profiles, further demonstrating their distinct conformational behavior. The 1IYT-derived peptide displayed pronounced changes in compactness throughout the trajectory. During the early simulation, Rg fluctuated considerably, followed by a period of conformational expansion during approximately 90-120 ns, when values reached approximately 1.4-1.5 nm. A marked decrease occurred at around 125 ns, after which Rg

remained predominantly close to 1.0 nm during much of the remaining trajectory. This transition indicates substantial compaction of 1IYT during the latter part of the simulation. Interestingly, the pronounced decrease in Rg for 1IYT occurred within approximately the same time window as the substantial increase in RMSD described in Section 3.2.1. The combination of a higher RMSD and lower Rg suggests that the peptide did not simply become increasingly disordered or expanded. Instead, it underwent a large-scale conformational rearrangement relative to its starting structure while adopting a more compact configuration. This observation illustrates the importance of interpreting RMSD together with complementary structural descriptors when evaluating highly dynamic peptides. The 1Z0Q-derived peptide exhibited rapid changes in compactness during the initial portion of the trajectory. Its Rg decreased from approximately 1.4 nm toward values around 1.0 nm, indicating early conformational compaction. This was followed by repeated expansion and contraction events throughout the simulation. Despite these fluctuations, 1Z0Q sampled relatively compact conformations during substantial portions of the trajectory, although transient increases in Rg indicate continued structural rearrangement rather than maintenance of a single compact state. The 6SZF-derived system displayed a different compactness profile. Following the initial structural adjustment, Rg generally fluctuated within approximately 1.1-1.3 nm over much of the trajectory. Compared with the compact conformations sampled by 1IYT during the later stages of the simulation, 6SZF therefore maintained a relatively more expanded global organization. Nevertheless, temporal fluctuations in Rg indicate continued changes in peptide dimensions throughout the 200-ns simulation. Overall, the Rg analysis demonstrates that the three Aβ42 conformers sampled distinct degrees and patterns of molecular compactness. The most pronounced transition was observed for 1IYT, where a relatively expanded intermediate state was followed by substantial late-stage compaction. In contrast, 1Z0Q underwent repeated transitions between more compact and expanded configurations, whereas 6SZF maintained a comparatively more expanded state during much of the

trajectory. Together with the RMSD and RMSF results, these findings demonstrate that the three experimentally derived starting conformations followed distinct global and local conformational pathways under identical simulation conditions.

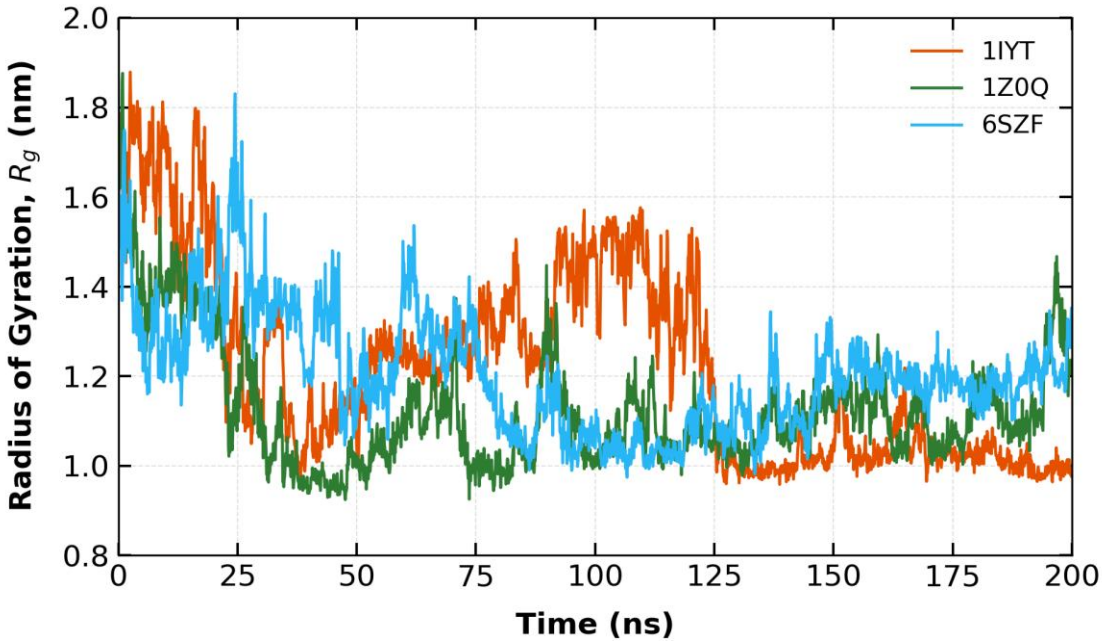


Fig. 4 Radius of gyration (Rg) profiles of Aβ42 during the 200-ns molecular dynamics simulations of 1IYT (orange), 1Z0Q (green), and 6SZF (cyan) systems as a function of simulation time

3.3. Secondary-structure dynamics of Aβ42

To further characterize the conformational behavior identified by the RMSD, RMSF, and Rg analyses, the secondary-structure evolution of Aβ42 was examined over the complete 200-ns trajectories using DSSP analysis (Fig. 5).

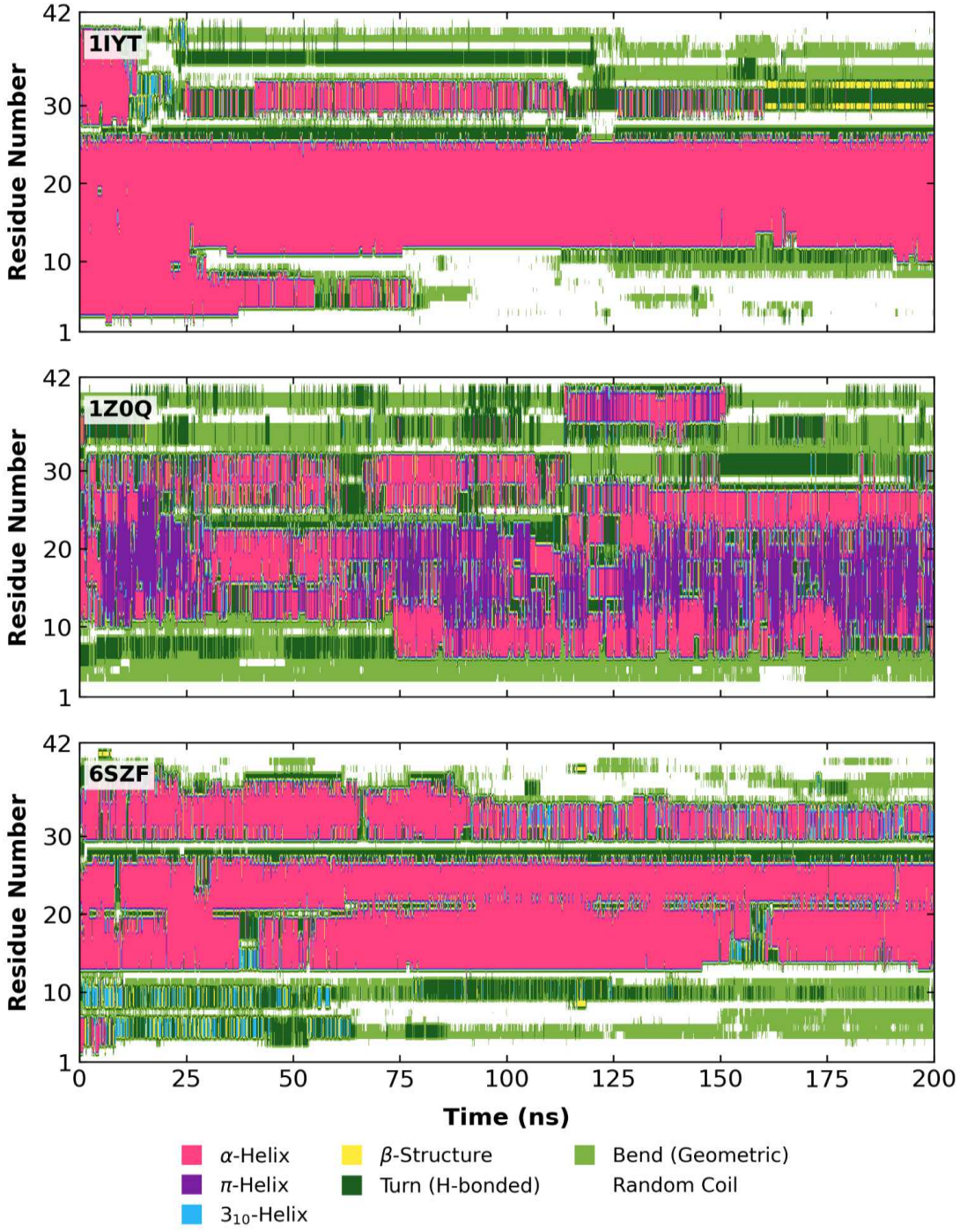


Fig. 5 Residue-wise DSSP assignments for the 1IYT-, 1Z0Q-, and 6SZF-derived Aβ42 systems over the complete 200-ns trajectories

The three systems exhibited markedly different secondary-structure distributions and temporal patterns despite being simulated under identical POPC-water conditions. The trajectory-averaged secondary-structure populations are summarized in Table 1, while the secondary-structure compositions of the corresponding starting PDB structures are included only as structural references.

Table 1. Secondary-structure composition of Aβ42 starting structures and 200-ns trajectories

Secondary structure (%)	1IYT PDB*	1IYT 200 ns	1Z0Q PDB*	1Z0Q 200 ns	6SZF PDB*	6SZF 200 ns
Turn	14.29	12.61	50.00	21.04	64.28	14.23
α-Helix	78.57	44.77	33.33	25.11	11.90	41.59
π-Helix	–	0.05	–	18.45	–	0.02
β-Bridge	–	0.69	–	–	–	0.13
Coil	7.14	26.66	7.14	14.43	16.66	26.77
3_{10}-Helix	–	0.54	9.52	0.13	7.14	3.42
Bend	–	11.60	–	20.83	–	11.89
PP helix	–	3.07	–	–	–	1.94

** Starting PDB secondary-structure compositions are provided for structural reference only. The 200-ns values represent secondary-structure populations calculated over the complete MD trajectories and do not represent the secondary structure of the final 200-ns frame.*

The 1IYT-derived peptide maintained a strong α-helical character throughout the simulation, with α-helix representing the dominant secondary-structure population at 44.77% over the 200-ns trajectory. Coil conformations constituted 26.66%, followed by turns (12.61%) and bends (11.60%). Smaller populations of polyproline-II-like helix (3.07%), β-bridge (0.69%), 3_{10}-helix (0.54%), and π-helix (0.05%) were also sampled. The time-resolved DSSP profile (Fig. 5) nevertheless showed substantial local rearrangement, indicating that the persistence of α-helical character did not correspond to maintenance of a rigid secondary-structure pattern throughout the trajectory. A considerably more

heterogeneous secondary-structure distribution was observed for 1Z0Q. α-Helical conformations accounted for 25.11% of the trajectory, while turns and bends represented 21.04% and 20.83%, respectively. Most notably, π-helical conformations constituted 18.45%, substantially exceeding the negligible π-helical populations observed for 1IYT and 6SZF. Coil structures contributed a further 14.43%, whereas 3_{10}-helix accounted for only 0.13%. The relatively balanced distribution among several structural classes, together with the frequent transitions visible in the DSSP map, indicates pronounced conformational heterogeneity within the 1Z0Q trajectory. The 6SZF-derived peptide exhibited α-helix as its predominant secondary-structure component, accounting for 41.59% of the trajectory. Coil conformations represented 26.77%, followed by turns (14.23%) and bends (11.89%). Smaller contributions were observed for 3_{10}-helix (3.42%) and polyproline-II-like helix (1.94%), whereas β-structure (0.13%) and π-helix (0.02%) remained minimally populated. This distribution is particularly notable when considered in relation to the fibril-derived starting configuration of 6SZF, which contained comparatively little α-helical structure. However, because the reported 200-ns percentages represent populations sampled across the entire trajectory rather than an endpoint structure, this observation should be interpreted as extensive sampling of α-helical conformations during the simulation rather than conversion to a single stable α-helical endpoint. Comparison of the three systems therefore revealed distinct conformational signatures over the 200-ns simulations. 1IYT and 6SZF both sampled substantial α-helical populations, although from very different starting conformations, whereas 1Z0Q exhibited the greatest structural heterogeneity and was distinguished by pronounced π-helical sampling. In all three systems, appreciable coil, turn, and bend populations further demonstrate the conformational plasticity of Aβ42 in the membrane-associated aqueous environment. These findings complement the global structural descriptors described above. The substantial RMSD changes cannot be attributed simply to loss of structural organization, because significant organized secondary structure persisted throughout all

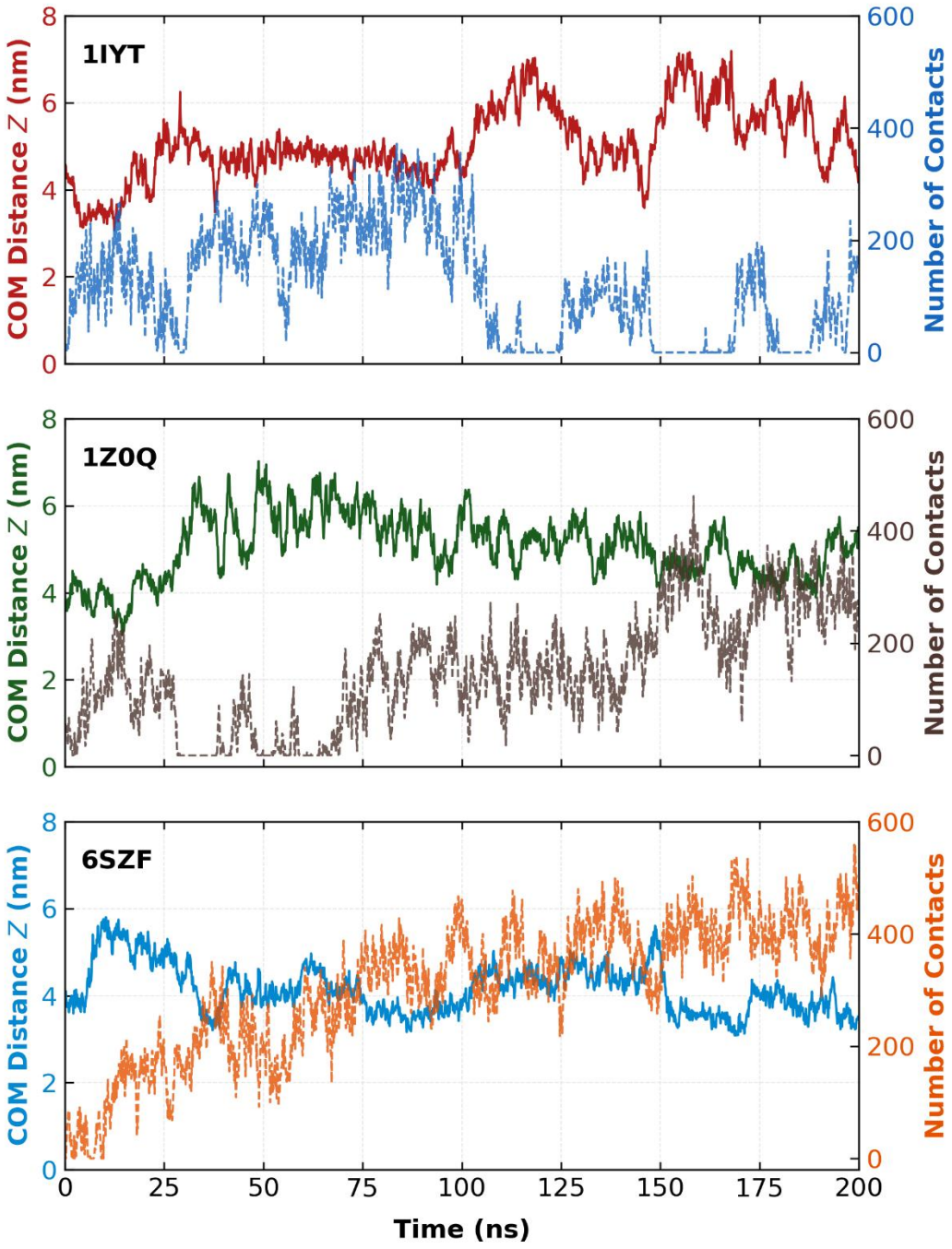
three trajectories. Instead, the combined RMSD, Rg, and DSSP results indicate redistribution among conformational states and remodeling of the peptide relative to its respective starting configuration. The differences among the three trajectories further support the importance of the initial conformational state in determining the structural landscape sampled by Aβ42 within the accessible 200-ns simulation timescale.

3.4. Conformation-dependent interaction of Aβ42 with the POPC membrane

Following characterization of the global and secondary-structure dynamics of Aβ42, the interaction of the three peptide conformers with the POPC bilayer was examined. Because each peptide was initially positioned in the aqueous phase above the upper membrane leaflet rather than embedded within the bilayer, the simulations allowed peptide-membrane association to develop without imposing an initially inserted configuration. The interaction behavior was evaluated using complementary descriptors, including the peptide center-of-mass position along the membrane-normal direction, the number of peptide-POPC contacts, hydrogen-bond formation, and residue-specific minimum distances from the membrane.

3.4.1. Coupled peptide-membrane position and contact dynamics

The temporal relationship between the position of Aβ42 relative to the membrane and its direct interaction with POPC was examined by comparing the peptide center-of-mass coordinate along the membrane-normal direction (COM Z-distance) with the number of peptide-lipid contacts (Fig. 6).



433

434 **Fig. 6** Coupled evolution of Aβ42 position along the membrane-normal direction and peptide-POPC
435 contacts during the 200-ns molecular dynamics simulations. Time-dependent center-of-mass coordinate
436 along the membrane-normal direction (COM Z-distance; solid lines, left axes) and number of Aβ42-
437 POPC contacts (dashed lines, right axes) for the 1IYT-, 1Z0Q-, and 6SZF-derived systems

The three systems displayed markedly different temporal profiles, indicating that the initial Aβ42 conformation influenced the subsequent mode and persistence of membrane association. For 1IYT, substantial changes in both COM Z-distance and peptide-POPC contacts occurred throughout the trajectory. During approximately the first 100 ns, the peptide maintained appreciable numbers of lipid contacts despite considerable fluctuations in its position along the membrane-normal direction. Contact numbers frequently reached approximately 200-300 during this period. After approximately 100 ns, however, the contact number decreased sharply and remained very low over several extended intervals. This reduction coincided with an increase in the COM Z-distance, which reached approximately 6-7 nm during parts of the second half of the trajectory. Although transient increases in contacts subsequently occurred, particularly around 125-145 and 165-175 ns, extensive contact with POPC was not continuously maintained. Thus, 1IYT exhibited a dynamic and intermittent membrane-association pattern, with substantial interaction during the earlier trajectory followed by periods of pronounced disengagement from the membrane interface. A different interaction pattern was observed for 1Z0Q. During the early trajectory, the COM Z-distance increased from approximately 4 nm to values approaching 6 nm, while the number of POPC contacts decreased to very low levels during approximately 30-65 ns. Contacts subsequently recovered and became increasingly prominent during the second half of the trajectory. In particular, after approximately 140 ns, contact numbers frequently reached approximately 250-400 while the COM Z-distance generally decreased toward approximately 4-5 nm. This temporal relationship indicates renewed and comparatively persistent interaction of 1Z0Q with the POPC membrane during the later stages of the simulation. The 6SZF-derived peptide exhibited the clearest progressive increase in peptide-POPC contacts. Contact numbers increased substantially during the early trajectory and, despite considerable fluctuations, continued to rise over the course of the simulation. During much of the second half of the trajectory, approximately 300-500 contacts were

observed. Meanwhile, the COM Z-distance remained predominantly within approximately 3-5 nm, with several positional rearrangements but without the prolonged large increase observed for 1IYT. By the later stages of the trajectory, 6SZF therefore exhibited extensive and persistent direct interaction with POPC. Comparison of the three systems reveals substantially different membrane-association pathways. 1IYT displayed the most intermittent interaction pattern, 1Z0Q underwent an initial period of reduced association followed by renewed contact formation, whereas 6SZF developed progressively extensive and persistent POPC contacts. These differences are particularly notable because the membrane composition and simulation conditions were identical among the three systems, indicating that the starting conformation of Aβ42 can influence the membrane-association pathway sampled within the 200-ns timescale. Importantly, the COM Z-distance and contact number provide related but non-equivalent information. The center-of-mass coordinate describes the global position of the peptide relative to the membrane-normal direction, whereas contact analysis reports direct spatial proximity between peptide and lipid atoms. Consequently, extensive lipid contacts may persist even when the peptide center of mass remains several nanometers from the membrane, depending on peptide orientation, extension, and the particular residues interacting with the bilayer. The combined analysis therefore provides a more informative description of membrane association than either descriptor considered independently. Residue-specific minimum-distance analysis presented below is used to identify which regions of Aβ42 contribute to these distinct interaction patterns.

3.4.2. Peptide-POPC hydrogen-bond analysis

To further characterize the molecular interactions underlying Aβ42 association with the POPC membrane, hydrogen bonds formed between the peptide and lipid molecules were monitored throughout the 200-ns trajectories (Fig. 7). In contrast to the contact analysis, which describes general spatial

association between Aβ42 and POPC, hydrogen-bond analysis provides a more specific measure of polar interactions at the peptide-membrane interface [McDonald and Thornton 1994]. Distinct temporal patterns were observed for the three starting conformations. The 1IYT-derived peptide exhibited intermittent hydrogen-bond formation with POPC. During the initial part of the trajectory, the number of hydrogen bonds was generally low, followed by a period of increased interaction between approximately 30 and 55 ns, during which as many as approximately six hydrogen bonds were observed. Hydrogen bonding remained detectable but more variable during approximately 60-105 ns, after which the frequency decreased substantially. During much of the second half of the trajectory, only isolated hydrogen-bonding events were observed, with extended periods in which no peptide-POPC hydrogen bonds were detected. This behavior is consistent with the contact analysis, which showed substantially reduced POPC association of 1IYT during large portions of the later trajectory. The 1Z0Q system displayed a notably different hydrogen-bonding pattern. Hydrogen bonding was limited during much of the early trajectory, apart from a transient increase around 20-25 ns. From approximately 70 ns onward, however, peptide-POPC hydrogen bonds became more frequent. The interaction strengthened further during the later portion of the simulation, particularly around 145-165 ns and again after approximately 175 ns, when multiple hydrogen bonds were frequently maintained. Counts reached approximately eight to nine during some intervals. The progressive increase in hydrogen bonding broadly corresponds to the recovery and subsequent increase in peptide-POPC contacts observed for 1Z0Q in Fig. 6, supporting enhanced interfacial association during the latter half of the simulation. The 6SZF-derived peptide exhibited the most pronounced increase in hydrogen-bond formation over the course of the simulation. Following relatively limited hydrogen bonding during the earliest portion of the trajectory, several peptide-POPC hydrogen bonds became established and persisted with substantial fluctuations. From approximately 100 ns onward, the number of hydrogen bonds generally increased, and during the final portion of the

trajectory values frequently ranged from approximately six to ten, with transient counts approaching 12 hydrogen bonds. This progressive behavior closely parallels the increasing number of peptide-POPC contacts observed for 6SZF, providing complementary evidence for persistent interaction of this conformer with the membrane interface. Taken together, the hydrogen-bond profiles reinforce the distinct membrane-association behaviors identified by the contact analysis. 1IYT exhibited predominantly transient hydrogen bonding followed by substantial loss of these interactions, whereas 1Z0Q developed increased hydrogen bonding during the later trajectory and 6SZF showed the clearest progressive establishment of persistent peptide-POPC hydrogen bonds. The agreement between the hydrogen-bond and contact profiles strengthens the interpretation that the three starting conformations follow different pathways of interaction with the same POPC membrane environment. Nevertheless, hydrogen-bond counts should not be interpreted as a direct quantitative measure of overall membrane-binding affinity. Peptide-membrane association can additionally involve electrostatic, van der Waals, and hydrophobic interactions that are not represented by hydrogen-bond counts alone. The present analysis therefore identifies hydrogen bonding as one component of the interfacial interaction network. The residue-specific proximity analysis in the following section provides additional spatial information regarding which regions of Aβ42 participate in membrane association.

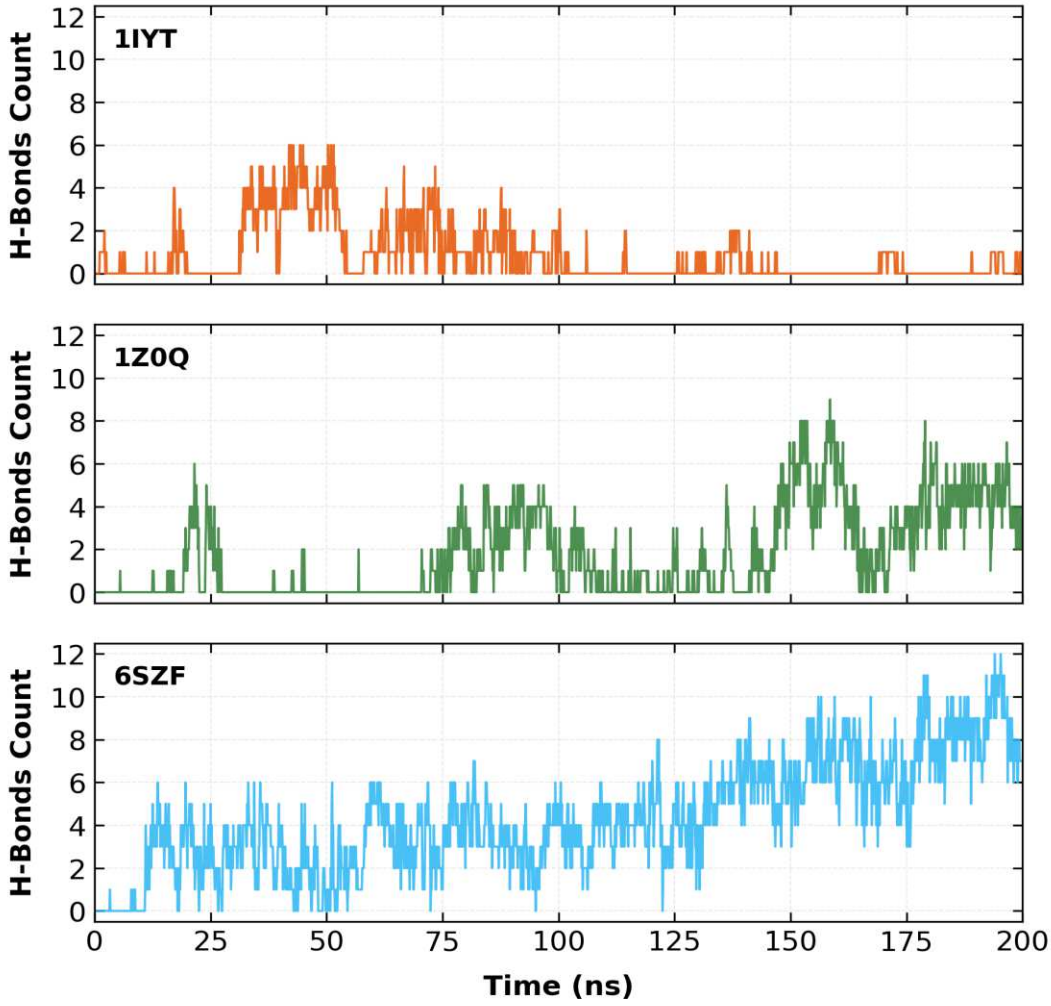


Fig. 7 Number of hydrogen bonds formed between Aβ42 and POPC molecules as a function of simulation time for 1IYT, 1Z0Q, and 6SZF systems

3.5. Residue-specific Aβ42-POPC interaction patterns

To identify which regions of Aβ42 contributed to membrane association, residue-specific minimum distances between the peptide and POPC were monitored throughout the complete 200-ns trajectories (Fig. 8). This analysis complements the global COM-position, contact, and hydrogen-bond measurements by resolving membrane proximity at the level of individual residues. Lower minimum-distance values indicate closer spatial proximity to POPC, whereas larger values indicate residues

positioned farther from the membrane. The resulting maps revealed pronounced differences among the three Aβ42 conformers in both the location and persistence of membrane-proximal regions. The 1IYT-derived peptide displayed a highly dynamic residue-specific interaction pattern. During the early part of the simulation, multiple regions of the peptide transiently approached the POPC membrane, indicating that membrane association was not restricted to a single persistent segment. Several residues within the N-terminal and central portions sampled relatively short distances during approximately the first 100 ns. However, after approximately 100-120 ns, much of the peptide exhibited larger minimum distances from POPC for extended periods, with only localized regions transiently returning to closer proximity. This change is consistent with the pronounced reduction in the total number of peptide-POPC contacts and hydrogen bonds observed during the latter part of the 1IYT trajectory. Thus, the apparent disengagement identified by the global interaction metrics is also evident at residue-level resolution. The 1Z0Q-derived peptide exhibited a substantially different spatial pattern. During the early and intermediate stages of the simulation, membrane proximity was heterogeneous, with individual sequence regions alternating between closer and more distant configurations. In the later portion of the trajectory, however, an increasing number of residues sampled shorter minimum distances from POPC. This behavior coincided with the increase in total peptide-lipid contacts and hydrogen-bond formation described above, indicating that the late-stage membrane association of 1Z0Q involved broader participation of the peptide sequence rather than being represented solely by movement of its center of mass. The most persistent residue-level membrane association was observed for 6SZF. Following the initial stage of the simulation, multiple regions of the peptide maintained relatively short minimum distances from POPC for extended periods. The map indicates sustained membrane proximity particularly across portions of the central and C-terminal regions, while other residues displayed greater temporal variability. Compared with 1IYT and 1Z0Q, the 6SZF trajectory therefore exhibited a broader and more persistent pattern of residue–lipid

proximity. This result agrees with the progressively increasing peptide-POPC contact number and hydrogen-bond formation observed for this system. Collectively, the minimum-distance analysis demonstrates that the differences among the three systems extend beyond changes in the global position of the peptide relative to the bilayer. Instead, each starting conformation produced a distinct residue-specific membrane-interaction pattern. The intermittent proximity observed for 1IYT, the development of broader membrane association during the later stages of 1Z0Q, and the comparatively persistent interaction of multiple 6SZF regions with POPC are consistent with the contact and hydrogen-bond analyses. The agreement among these independent descriptors provides stronger evidence for conformation-dependent membrane association than any single metric considered in isolation. These findings are also relevant to the conformational behavior described in Sections 3.2 and 3.3. Because different sequence regions experience different degrees of membrane proximity, the POPC interface provides a spatially heterogeneous environment for Aβ42 rather than constraining the peptide uniformly. However, the present simulations establish an association between membrane interaction and conformational evolution rather than direct causality. Determining whether specific lipid contacts directly drive individual secondary-structure transitions would require additional analyses or simulations specifically designed to resolve such coupling.

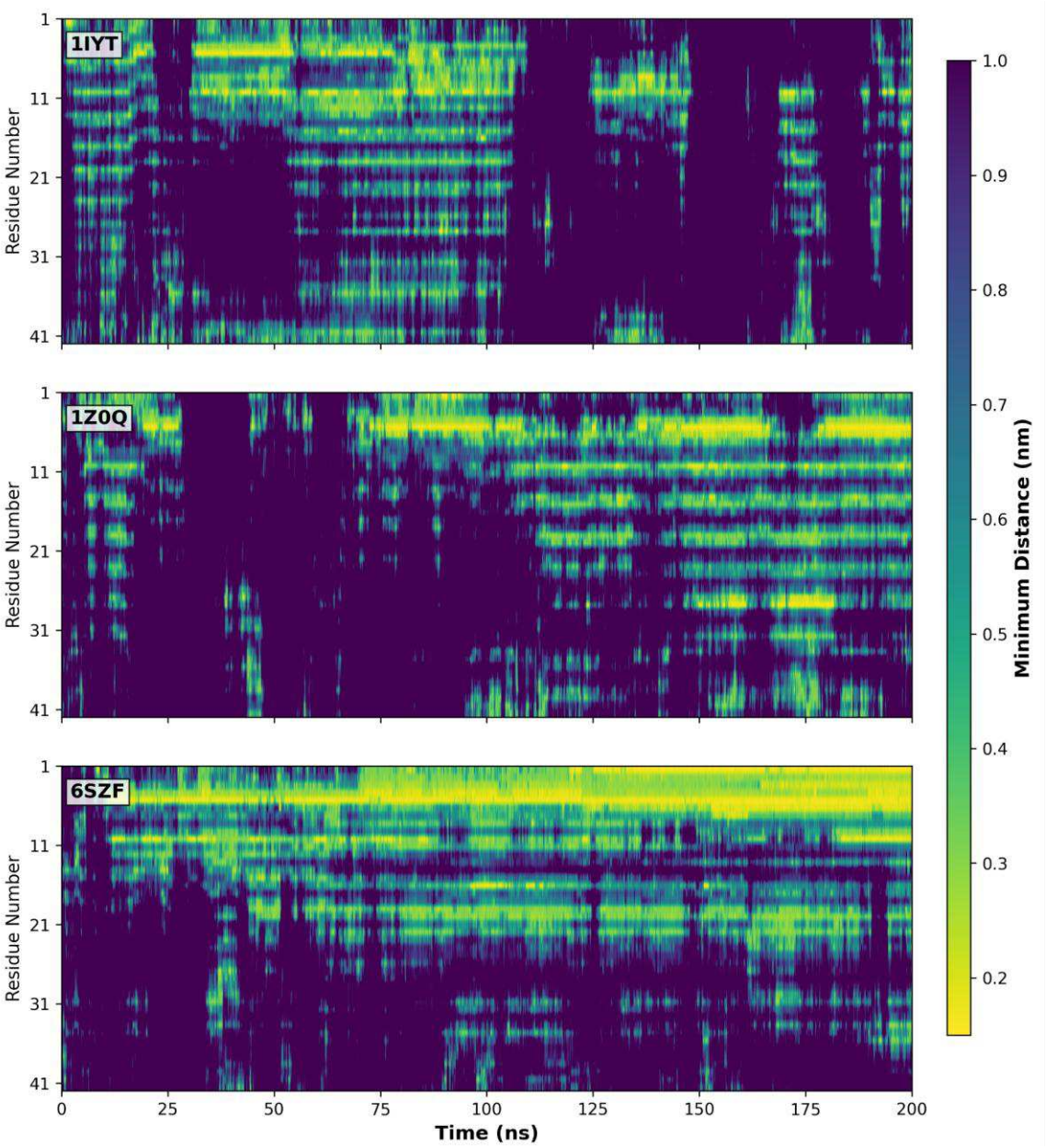


Fig. 8 Residue-specific minimum-distance maps describing Aβ42-POPC membrane interactions during the 200-ns molecular dynamics simulations for the 1IYT, 1Z0Q, and 6SZF systems

3.6. Residue-specific solvent accessibility of Aβ42

To characterize how the different starting conformations influenced the exposure of individual Aβ42 residues to the surrounding solvent, residue-specific solvent-accessible surface area (SASA) was

monitored throughout the complete 200-ns trajectories (Fig. 9). Residue-resolved analysis provides spatial information on the distribution of solvent exposure along the peptide sequence and allows persistent or transient changes in accessibility to be distinguished among the three conformational states (Connolly 1983; Lee and Richards 1971). The 1IYT-derived peptide displayed pronounced heterogeneity in solvent accessibility along its sequence. Several residues within the N-terminal region maintained comparatively high SASA values over substantial portions of the trajectory, indicating persistent exposure to the aqueous environment. In contrast, much of the central region exhibited lower accessibility. The temporal pattern also changed during the simulation, particularly after approximately 120-150 ns, when several sequence regions underwent clear alterations in their exposure profiles. These changes coincide broadly with the major conformational rearrangement identified by the RMSD and Rg analyses, supporting substantial redistribution of residue exposure as 1IYT adopted a structurally distinct ensemble during the latter part of the trajectory. The 1Z0Q-derived peptide exhibited a more heterogeneous and temporally variable SASA pattern. Alternating regions of relatively high and low accessibility were distributed throughout the sequence, and several residues underwent repeated changes in solvent exposure during the simulation. Particularly noticeable temporal reorganizations occurred within both the central and C-terminal portions of the peptide. This heterogeneous exposure pattern is consistent with the substantial conformational diversity identified by DSSP analysis, where 1Z0Q sampled multiple secondary-structure classes rather than remaining dominated by a single structural motif. For the 6SZF-derived peptide, the residue-specific SASA map showed a comparatively persistent pattern of solvent exposure across several sequence regions. The N-terminal portion contained residues with consistently high accessibility, while portions of the central sequence exhibited lower SASA values. Several C-terminal residues also underwent time-dependent changes in exposure. Importantly, considerable solvent accessibility persisted despite the extensive peptide-POPC contacts and hydrogen-bond formation observed for this system.

This indicates that membrane association did not result in uniform shielding of the peptide from the aqueous environment. Comparison of the three systems therefore demonstrates that membrane-associated Aβ42 retains a highly heterogeneous solvent-exposure landscape, with accessibility determined by both residue position and the conformational state sampled during the trajectory. The distinct temporal patterns further indicate that solvent exposure is dynamically redistributed as Aβ42 undergoes structural rearrangement and interaction with the membrane interface. When considered together with the residue-specific membrane-distance analysis, these results provide complementary descriptions of the local environment experienced by individual peptide regions. Residues positioned close to POPC are not necessarily completely inaccessible to solvent, because membrane association can involve only part of a residue or peptide segment while other molecular surfaces remain exposed to water. Thus, the combined residue-level analyses support a model in which Aβ42 interacts with the membrane through spatially heterogeneous and dynamically reorganizing interfaces, rather than undergoing uniform burial at the lipid surface.

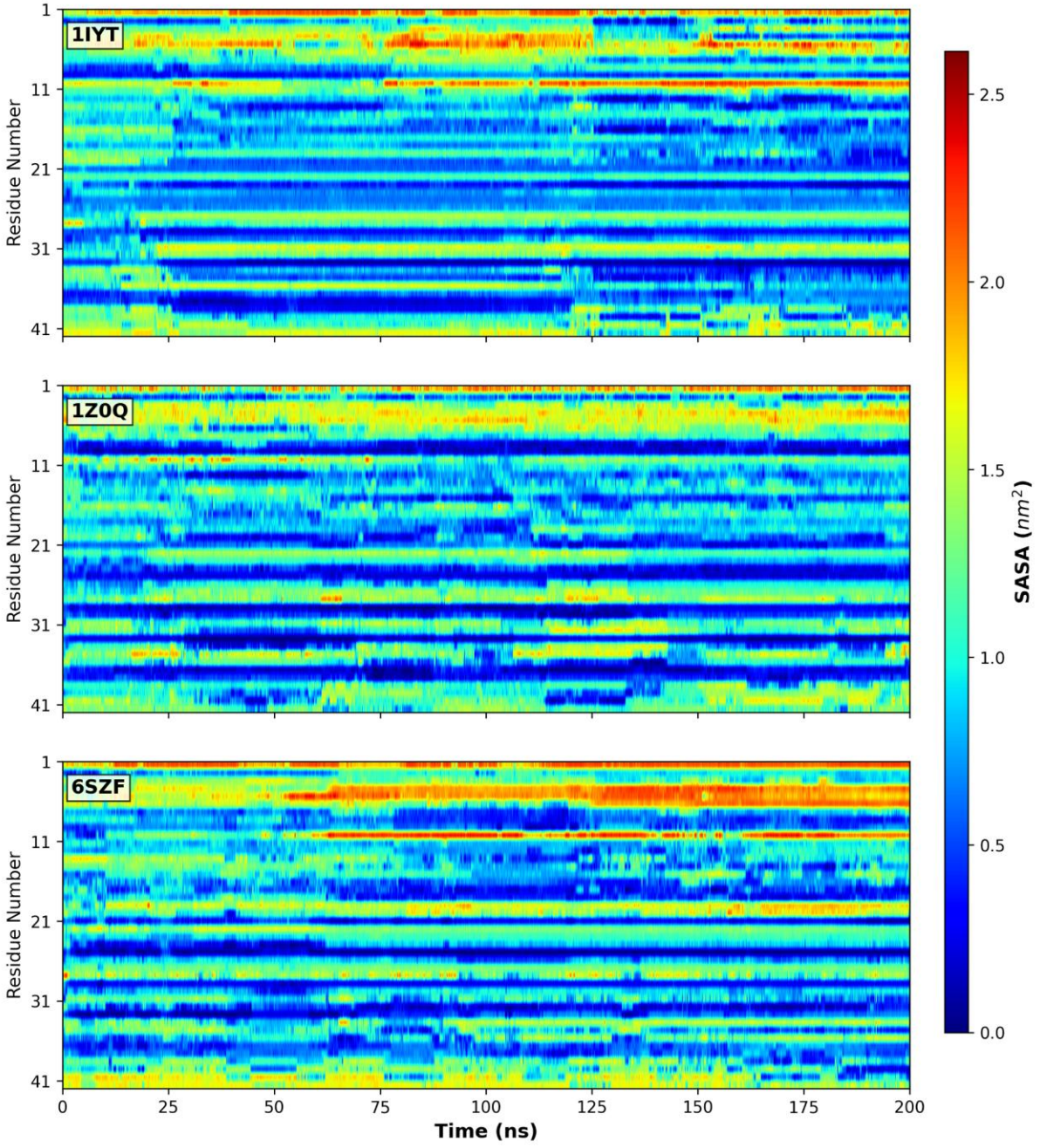


Fig. 9 Time-resolved residue-specific solvent-accessible surface area (SASA) of Aβ42 during the 200-ns molecular dynamics simulations for the 1IYT, 1Z0Q, and 6SZF systems

4. Conclusion

This study demonstrates that the initial conformational state of amyloid-β42 strongly influences the structural and membrane-association pathways sampled in a POPC-water environment. Comparative 200-ns molecular dynamics simulations of three experimentally derived Aβ42 structures (1IYT, 1Z0Q, and 6SZF) revealed distinct behaviors across global conformational dynamics, secondary-structure evolution, peptide-lipid interactions, residue-specific membrane proximity, and solvent accessibility. The 1IYT-derived peptide underwent pronounced conformational remodeling and late-stage compaction, accompanied by increasingly intermittent POPC interactions. 1Z0Q exhibited greater conformational heterogeneity and evolved from relatively limited early membrane association toward enhanced peptide-lipid contacts and hydrogen bonding during the later trajectory. In contrast, 6SZF developed the most persistent POPC interaction pattern, characterized by extensive lipid contacts and increasing hydrogen bonding while retaining substantial residue-specific solvent exposure. These observations demonstrate that membrane association does not necessarily require global peptide compaction or uniform solvent shielding. Collectively, the results indicate that structurally distinct Aβ42 conformers can follow markedly different interaction pathways even when exposed to identical membrane and simulation conditions. The study therefore highlights the importance of starting-structure diversity when modeling flexible and aggregation-prone peptides, since simulations based on a single structure may capture only a subset of accessible behaviors. Although the present trajectories do not define equilibrium populations or binding free energies, they provide an atomistic framework for understanding the conformational heterogeneity of membrane-associated Aβ42 and motivate future ensemble and free-energy studies of Aβ42-lipid recognition.

Statements and Declarations

Funding

This work was supported by the JINR project "Nanobiophotonics" (# 1147-1).

Competing Interest Statement

The authors have no relevant financial or non-financial interests to disclose.

Author Contributions

All authors contributed to the study conception and design. Investigation, data collection, visualization, analysis and writing an original draft were performed by Yersultan Arynbek, Khlood A.A. Abdeljawaad and Duc Huy Le. Supervision, investigation, review and editing were performed by Kahramon Mamatkulov and Grigory Arzumanyan. All authors read and approved the final manuscript.

Data Availability

The datasets generated during and/or analysed during the current study are available from the corresponding author on reasonable request.

References

Abdeljawaad KAA, Arynbek Y, Mamatkulov K, Duc Le H, Ibrahim MAA, Mekhemer GAH, Arzumanyan G (2026) pH modulates amyloid-β42 conformation in lipid membranes: evidence from circular dichroism, Raman spectroscopy, and molecular dynamics simulations. Journal of Biomolecular Structure and Dynamics 44:5189-5204

Abraham MJ, Murtola T, Schulz R, Páll S, Smith JC, Hess B, Lindahl E (2015) GROMACS: High performance molecular simulations through multi-level parallelism from laptops to supercomputers. SoftwareX 1-2:19-25

662 Anikina A, Belyakov D, Bezhanyan T, Kirakosyan M, Kokorev A, Lyubimova M, Matveev M,
663 Podgainy D, Rahmonova A, Shadmehri S, Streltsova O, Torosyan S, Vala M, Zuev M (2025)
664 Structure and Features of the Software and Information Environment of the HybriLIT
665 Heterogeneous Platform. In: Vishnevsky VM, Samouylov KE, Kozyrev DV (eds) Distributed
666 Computer and Communication Networks. Springer Nature Switzerland, Cham, pp 444-457

667 Banerjee S, Hashemi M, Zagorski K, Lyubchenko YL (2020) Interaction of Aβ42 with Membranes
668 Triggers the Self-Assembly into Oligomers. International journal of molecular sciences 21

669 Benson NC, Daggett V (2008) Dynameomics: large-scale assessment of native protein flexibility.
670 Protein science : a publication of the Protein Society 17:2038-2050

671 Berman HM, Westbrook J, Feng Z, Gilliland G, Bhat TN, Weissig H, Shindyalov IN, Bourne PE
672 (2000) The Protein Data Bank. Nucleic acids research 28:235-242

673 Bernetti M, Bussi G (2020) Pressure control using stochastic cell rescaling. The Journal of Chemical
674 Physics 153:114107

675 Bundschuh BF, Kley F, Fatafta H, Strodel B (2026) All-atom MD simulations of amyloid-membrane
676 interactions: Setup, execution, and analysis. Methods in enzymology 729:389-417

677 Bussi G, Donadio D, Parrinello M (2007) Canonical sampling through velocity rescaling. The Journal
678 of Chemical Physics 126:014101

679 Butterfield SM, Lashuel HA (2010) Amyloidogenic protein-membrane interactions: mechanistic
680 insight from model systems. Angewandte Chemie (International ed in English) 49:5628-5654

Connolly ML (1983) Analytical molecular surface calculation. Journal of Applied Crystallography 16:548-558

Crescenzi O, Tomaselli S, Guerrini R, Salvadori S, D'Ursi AM, Temussi PA, Picone D (2002) Solution structure of the Alzheimer amyloid β-peptide (1–42) in an apolar microenvironment. European Journal of Biochemistry 269:5642-5648

Davis CH, Berkowitz ML (2009) Interaction between amyloid-beta (1-42) peptide and phospholipid bilayers: a molecular dynamics study. Biophysical journal 96:785-797

Esawii HA, Arynbek Y, Mohamed N, Arzumanyan G, Mahran HA (2025) A Molecular Dynamics Investigation into Optimum Membrane-Cholesterol Performance Influencing Alzheimer's-Related Amyloid-β Conformational Stability. Advanced Theory and Simulations 8:2500180

Gorelov S, Titov A, Tolicheva O, Konevega A, Shvetsov A (2024) DSSP in GROMACS: Tool for Defining Secondary Structures of Proteins in Trajectories. Journal of chemical information and modeling 64:3593-3598

Hardy J, Selkoe DJ (2002) The amyloid hypothesis of Alzheimer's disease: progress and problems on the road to therapeutics. Science (New York, NY) 297:353-356

Hess B, Bekker H, Berendsen HJC, Fraaije JGEM (1997) LINCS: A linear constraint solver for molecular simulations. Journal of computational chemistry 18:1463-1472

Huang J, Rauscher S, Nawrocki G, Ran T, Feig M, de Groot BL, Grubmüller H, MacKerell AD (2017) CHARMM36m: an improved force field for folded and intrinsically disordered proteins. Nature Methods 14:71-73

Humphrey W, Dalke A, Schulten K (1996) VMD: visual molecular dynamics. Journal of molecular graphics 14:33-38, 27-38

Jo S, Kim T, Iyer VG, Im W (2008) CHARMM-GUI: a web-based graphical user interface for CHARMM. Journal of computational chemistry 29:1859-1865

Jo S, Lim JB, Klauda JB, Im W (2009) CHARMM-GUI Membrane Builder for mixed bilayers and its application to yeast membranes. Biophysical journal 97:50-58

Jorgensen WL, Chandrasekhar J, Madura JD, Impey RW, Klein ML (1983) Comparison of simple potential functions for simulating liquid water. The Journal of Chemical Physics 79:926-935

Kabsch W, Sander C (1983) Dictionary of protein secondary structure: Pattern recognition of hydrogen-bonded and geometrical features. Biopolymers 22:2577-2637

Lee B, Richards FM (1971) The interpretation of protein structures: estimation of static accessibility. Journal of molecular biology 55:379-400

Maiorov VN, Crippen GM (1994) Significance of Root-Mean-Square Deviation in Comparing Three-dimensional Structures of Globular Proteins. Journal of molecular biology 235:625-634

Mamatkulov K, Zavatski S, Arynbek Y, Esawii HA, Burko A, Bandarenka H, Arzumanyan G (2025) Conformational analysis of lipid membrane mimetics modified with Aβ42 peptide by Raman spectroscopy and computer simulations. Journal of Biomolecular Structure and Dynamics 43:9994-10007

Matsuzaki K (2007) Physicochemical interactions of amyloid β-peptide with lipid bilayers. Biochimica et Biophysica Acta (BBA) - Biomembranes 1768:1935-1942

McDonald IK, Thornton JM (1994) Satisfying Hydrogen Bonding Potential in Proteins. Journal of molecular biology 238:777-793

Mrdenovic D, Pieta IS, Nowakowski R, Kutner W, Lipkowski J, Pieta P (2022) Amyloid β interaction with model cell membranes – What are the toxicity-defining properties of amyloid β? International Journal of Biological Macromolecules 200:520-531

Nguyen PH, Derreumaux P (2023) Recent Computational Advances Regarding Amyloid-β and Tau Membrane Interactions in Alzheimer's Disease. Molecules (Basel, Switzerland) 28

Poojari C, Kukol A, Strodel B (2013) How the amyloid-β peptide and membranes affect each other: An extensive simulation study. Biochimica et Biophysica Acta (BBA) - Biomembranes 1828:327-339

Santoro A, Grimaldi M, Buonocore M, Stillitano I, D'Ursi AM (2021) Exploring the Early Stages of the Amyloid Aβ(1–42) Peptide Aggregation Process: An NMR Study Pharmaceuticals, vol 14, pp 732

Sciacca MF, Kotler SA, Brender JR, Chen J, Lee DK, Ramamoorthy A (2012) Two-step mechanism of membrane disruption by Aβ through membrane fragmentation and pore formation. Biophysical journal 103:702-710

Selkoe DJ, Hardy J (2016) The amyloid hypothesis of Alzheimer's disease at 25 years. EMBO molecular medicine 8:595-608

Simmonett AC, Brooks BR (2021) A compression strategy for particle mesh Ewald theory. J Chem Phys 154:054112

741 Tofoleanu F, Buchete NV (2012) Molecular interactions of Alzheimer's Aβ protofilaments with lipid
742 membranes. Journal of molecular biology 421:572-586

743 Tomaselli S, Esposito V, Vangone P, van Nuland NAJ, Bonvin AMJJ, Guerrini R, Tancredi T,
744 Temussi PA, Picone D (2006) The α-to-β Conformational Transition of Alzheimer's Aβ-(1–42)
745 Peptide in Aqueous Media is Reversible: A Step by Step Conformational Analysis Suggests the
746 Location of β Conformation Seeding. ChemBioChem 7:257-267

747 Torrens-Fontanals M, Stepniewski TM, Aranda-García D, Morales-Pastor A, Medel-Lacruz B, Selent J
748 (2020) How Do Molecular Dynamics Data Complement Static Structural Data of GPCRs.
749 International journal of molecular sciences 21

750 Weber OC, Uversky VN (2017) How accurate are your simulations? Effects of confined aqueous
751 volume and AMBER FF99SB and CHARMM22/CMAP force field parameters on structural
752 ensembles of intrinsically disordered proteins: Amyloid-β42 in water. Intrinsically Disordered
753 Proteins 5:e1377813

754 Williams TL, Serpell LC (2011) Membrane and surface interactions of Alzheimer's Aβ peptide--
755 insights into the mechanism of cytotoxicity. The FEBS journal 278:3905-3917
756